



# Evaluation method of the degree of red blood cell aggregation considering ultrasonic propagation attenuation by analyzing ultrasonic backscattering properties

Kanta Nagasawa<sup>1</sup> · Akiyo Fukase<sup>1</sup> · Shohei Mori<sup>2</sup> · Mototaka Arakawa<sup>1,2</sup> · Satoshi Yashiro<sup>3</sup> · Yasushi Ishigaki<sup>3</sup> · Hiroshi Kanai<sup>1,2</sup>

Received: 21 February 2020 / Accepted: 13 October 2020 / Published online: 12 January 2021

© The Japan Society of Ultrasonics in Medicine 2021

## Abstract

**Purpose** Red blood cell (RBC) aggregation is one of the main factors that determines blood viscosity and an important indicator for evaluating blood properties. As a noninvasive and quantitative method for diagnosing blood properties, our research group estimated the size of RBC aggregates by fitting the scattered power spectrum from the blood vessel lumen with the theoretical scattering characteristics to evaluate the degree of RBC aggregation. However, it was assumed that the propagation attenuation of ultrasound in the vascular lumen was the same regardless of whether RBCs were aggregated or not, which caused systematic errors in the estimated size.

**Methods** To improve the size estimation accuracy, we calculated and corrected the attenuation of the blood vessel lumen during RBC aggregation and non-aggregation. The attenuation in the blood vessel lumen was calculated with the spectra acquired from two different depths.

**Results** In the basic experiments using microparticles, the estimation accuracy decreased as the concentration increased in the case of the conventional method, but the estimated size tended to approach the true size irrespective of the concentration, removing the propagation attenuation component with the proposed method. In the in vivo experiment on the human hand dorsal vein, the size was estimated to be larger during RBC aggregation and smaller during non-aggregation using the proposed method.

**Conclusion** These results suggest that the proposed method can provide precise size estimation by considering the propagation attenuation component regardless of differences in blood conditions such as RBC concentration and degree of aggregation.

**Keywords** Ultrasound scattering · Red blood cells · Aggregation · Attenuation

## Introduction

Evaluation of blood properties is useful for early detection of cardiovascular diseases, and one of the main indicators is the degree of red blood cell (RBC) aggregation [1, 2]. RBC

aggregation is a reversible phenomenon among RBCs, and it is likely to occur when the blood flow is at a low shear rate. The degree of RBC aggregation is one of the factors that determines blood viscosity, and it has been reported to be related to other blood properties [3]. Conventional evaluation methods of blood properties are mainly based on the sampling of blood, which is invasive. Therefore, we have investigated a noninvasive and quantitative evaluation method of the blood properties based on calculating the degree of aggregation from the scattering properties of RBCs using ultrasound. RBCs are the main component of blood. There have been several reports on the evaluation of scattering properties from RBCs [4, 5]. Several studies have been reported on the evaluation of blood properties using ultrasound. Shung et al. observed changes in the brightness of blood echoes during a cardiac cycle [6, 7], and Patat et al.

✉ Mototaka Arakawa  
arakawa@ecei.tohoku.ac.jp

<sup>1</sup> Graduate School of Biomedical Engineering, Tohoku University, Sendai 980-8579, Japan

<sup>2</sup> Graduate School of Engineering, Tohoku University, Sendai 980-8579, Japan

<sup>3</sup> Division of Diabetes, Metabolism and Endocrinology, Department of Internal Medicine, Iwate Medical University, Yahaba, Iwate 028-3695, Japan

observed sound velocity and scatterer size changes during blood coagulation using human whole blood in vitro [8, 9]. All of these evaluation methods were applied to blood drawn by blood sampling, so these are invasive.

As a noninvasive method, in our research group, Saito et al. regarded the aggregated RBCs as a sphere scatterer in in vivo measurements, estimated the scatterer size by analyzing ultrasound scattering properties, and evaluated the degree of RBC aggregation [10, 11]. Kurokawa et al. proposed a selection of analysis beams in the detection of reflected waves from the posterior wall of a blood vessel, thereby improving the reproducibility of the reflected spectrum [12]. They also confirmed a clear difference in the estimated size before and during avascularization in in vivo measurements. However, the difference in the propagation attenuation component due to the difference in the ultrasonic propagation paths between the acquisitions of the power spectra from the lumen and the back wall of the blood vessel as a reference was not considered in their method. This caused a systematic error in the size estimation results. In fact, the deterioration of the estimation accuracy was confirmed as the particle size and the particle concentration increased in the basic experiments using microparticles. There are individual differences from 30 to 50% in the hematocrit (volume ratio of RBCs in the blood) [13], so it is necessary to consider the propagation attenuation component.

There have been several reports on the measurement of propagation attenuation in vivo. In the time domain, Baldwin et al. estimated myocardial attenuation using M-mode images [14], and Chen et al. estimated liver attenuation using harmonic imaging (HMI) [15]. In the frequency domain, there are estimation methods of attenuation using the downshift of the center frequency and the spectral difference [16]. Heo et al. estimated the attenuation of soft tissues by calculating the block power spectrum [17]. Kuc et al. estimated the attenuation using the difference in the slope of the logarithmic power spectra for two echo signals obtained from different depths in a tissue [18].

In the present study, we derived intravascular ultrasound propagation attenuation to estimate the size of RBCs in consideration of ultrasound propagation attenuation. Furthermore, we attempted to improve the accuracy of the size estimation method by correcting the propagation attenuation components.

## Materials and methods

### Measurement of ultrasonic backscatter properties

When the scatterer size is sufficiently smaller than the wavelength of the incident ultrasound, the scattering property follows Rayleigh scattering, and the scattering power is

proportional to the fourth power of the frequency. As the scatterer size increases, the frequency dependence of the scattered power becomes smaller.

Figure 1a, b shows the schematic diagrams of acquisition of RF signals scattered from RBCs to obtain the scattered power spectrum  $P_s(f, d_0)$  and those reflected from a posterior wall of the vein to obtain the reflected power spectrum  $P_r(f, d_0)$ , respectively.  $f$  is the frequency and  $d_0$  is the distance from the probe to the data acquisition position. Ultrasound is transmitted to blood vessels through water, gel, and epidermis. The focal point of the ultrasonic probe was set on the center of the vessel lumen in Fig. 1a and on the posterior wall of the vessel in Fig. 1b. Equations (1) and (2) show the power spectra  $P_s(f, d_0)$  scattered from the RBCs in the lumen of the blood vessel and  $P_r(f, d_0)$  reflected from the posterior wall of the vein, respectively. The measurement positions of both spectra are set at the same distance from the probe so that the sound pressure properties  $H(f, d_0)$  are equal:

$$P_s(f, d_0) = \left| S(f, d_0) G(f) A_s(f, d_0) H(f, d_0) X(f) \right|^2, \quad (1)$$

$$P_r(f, d_0) = \left| R \cdot G(f) A_r(f, d_0) H(f, d_0) X(f) \right|^2. \quad (2)$$

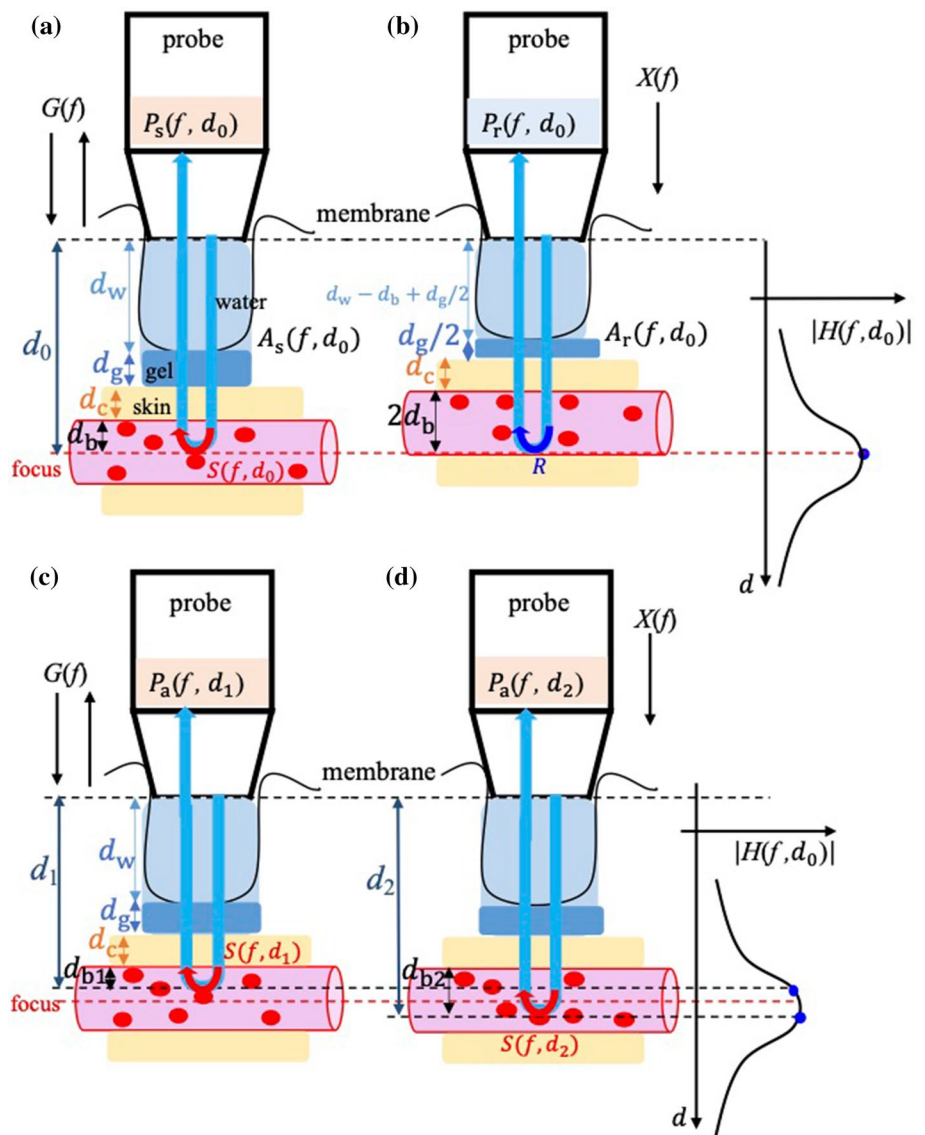
In addition to the scattering property from the RBCs  $S(f, d_0)$ , the scattered power spectrum from RBCs  $P_s(f, d_0)$  includes the transmission/reception property of the transducer  $G(f)$ , the sound pressure property of the ultrasonic probe  $H(f, d_0)$ , the frequency property of the applied signal  $X(f)$ , and the propagation attenuation property  $A_s(f, d_0)$ .  $P_r(f, d_0)$  includes  $R$  and  $A_r(f, d_0)$ , not  $S(f, d_0)$  and  $A_s(f, d_0)$ , respectively.  $R$  represents the reflection coefficient from the posterior wall of the blood vessel, and it has no frequency dependence.  $A_r(f, d_0)$  and  $A_s(f, d_0)$  are the propagation attenuation properties when acquiring the scattered wave from the RBC and the reflected wave from the back wall of the blood vessel, respectively.

To extract only the required scattering property  $S(f, d_0)$ ,  $P_s(f, d_0)$  is normalized by the reflected spectrum  $P_r(f, d_0)$  from a posterior wall of the vein, as shown in the following equation:

$$\begin{aligned} 10 \log_{10} \frac{P_s(f, d_0)}{P_r(f, d_0)} &= 10 \log_{10} \frac{\left| S(f, d_0) G(f) A_s(f, d_0) H(f, d_0) X(f) \right|^2}{\left| R \cdot G(f) A_r(f, d_0) H(f, d_0) X(f) \right|^2} \\ &\approx 10 \log_{10} \frac{\left| S(f, d_0) \right|^2}{|R|^2} + 10 \log_{10} \frac{\left| A_s(f, d_0) \right|^2}{\left| A_r(f, d_0) \right|^2}. \end{aligned} \quad (3)$$

Since the sound pressure property  $H(f, d_0)$ , the applied signal  $X(f)$ , and the transmission/reception characteristic  $G(f)$

**Fig. 1** Schematic diagrams of acquisitions of RF signals when acquiring scattered or reflected waves. **a**  $P_s(f, d_0)$  from the lumen (before avascularization). **b**  $P_r(f, d_0)$  from the rear wall. **c**  $P_a(f, d_1)$  from depth  $d_1$ . **d**  $P_a(f, d_2)$  from depth  $d_2$



are equal, these components are canceled by the normalization shown in Eq. (3). Furthermore, for the conventional method [10–12], the attenuation in each measurement in Fig. 1a, b was assumed to be equal, which means  $A_s(f, d_0) = A_r(f, d_0)$ , and the second term on the right side of Eq. (2) was considered to be 0. Then,  $10 \log_{10} \left( \frac{|S(f, d_0)|^2}{|R|^2} \right)$  was obtained from  $10 \log_{10} \{ P_s(f, d_0) / P_r(f, d_0) \}$ . However, the focal positions in the two measurements are different. Therefore, the intravascular ultrasound propagation paths are different from each other, as shown in Fig. 1a, b, and it is considered that the above assumption is not strict.  $A_w(f, d)$ ,  $A_g(f, d)$ ,  $A_s(f, d)$ , and  $A_b(f, d)$  are the attenuation properties of propagation in water, ultrasonic gel, skin, and blood before avascularization, respectively. In general, the propagation attenuation property  $A(f, d)$  can be expressed as  $A(f, d) = e^{-2\alpha(f)d}$  with

the attenuation coefficient  $\alpha(f)$  and the propagation distance  $d$ .

The propagation paths in water, ultrasonic gel, skin, and blood vessels when acquiring scattered waves from RBCs are  $d_w$ ,  $d_g$ ,  $d_s$ , and  $d_b$ , respectively. The attenuation components  $|A_s(f, d_0)|^2$  and  $|A_r(f, d_0)|^2$  are represented as Eqs. (4) and (5), respectively, as the sum of the attenuation components in water, gel, skin, and the lumen of the blood vessel:

$$|A_s(f, d_0)|^2 = |A_w(f, d_w)A_g(f, d_g)A_s(f, d_s)A_b(f, d_b)|^2, \quad (4)$$

$$|A_r(f, d_0)|^2 = |A_w(f, d_w - d_b + d_g/2)A_g(f, d_g/2)A_s(f, d_s)A_b(f, 2d_b)|^2. \quad (5)$$

When the reflected wave from the posterior wall is acquired, the propagation distance in the blood vessel is twice that when the scattered wave from the lumen is acquired, but the propagation distances in water and gel are shortened accordingly. Therefore, the total propagation distance  $d_0$  is equal in the two measurements. The propagation attenuation component  $10 \log_{10} \left| \frac{A_S(f, d_0)}{A_r(f, d_0)} \right|^2$  of the second term on the right side of Eq. (3) is obtained as follows:

$$10 \log_{10} \frac{\left| \frac{A_S(f, d_0)}{A_r(f, d_0)} \right|^2}{\left| \frac{A_S(f, d_0)}{A_r(f, d_0)} \right|^2} = 10 \log_{10} \left| \frac{A_S(f, d_0)}{A_r(f, d_0)} \right|^2 - 10 \log_{10} \left| \frac{A_S(f, d_0)}{A_r(f, d_0)} \right|^2$$

$$= 17.37 \left[ d_b \{ \alpha_b(f) - \alpha_w(f) \} + \frac{d_g}{2} \{ \alpha_w(f) - \alpha_g(f) \} \right], \tag{6}$$

where  $\alpha_b(f)$  is the attenuation coefficient of blood before avascularization and  $\alpha_w(f)$  is the attenuation coefficient of water. We insert the measured distance from the B-mode image into  $d_b$  and the published data  $\alpha_w(f) = 1.94 \times 10^{-16} \times f^2$  (dB/mm) (at 23 °C) [19] into  $\alpha_w(f)$ .  $\alpha_g(f)$  is the attenuation coefficient of gel. It is calculated from the difference in the amplitude spectra of the reflected waves from the same phantom when the medium of the ultrasonic wave propagation paths are changed with water and gel, referring to the published data of  $\alpha_w(f)$  [19]. Therefore, if the attenuation coefficient  $\alpha_b(f)$  of the blood can be obtained, the propagation attenuation component  $10 \log_{10} \left| \frac{A_S(f, d_0)}{A_r(f, d_0)} \right|^2$  that occurred during normalization in Eq. (3) can be calculated and removed.

**Calculation of blood attenuation coefficient  $\alpha_b(f)$ ,  $\alpha_b'(f)$**

To calculate the attenuation coefficients of blood before avascularization ( $\alpha_b(f)$ ) and during avascularization ( $\alpha_b'(f)$ ), we consider calculating the power spectra from different depths  $d_1$  and  $d_2$  ( $d_1 < d_0 < d_2$ ,  $d_0$  : focus), as shown in Fig. 1c, d.  $d_1$  and  $d_2$  are made an equal distance from the center of the lumen to reduce the difference in the RBC aggregation sizes caused by the distribution of the blood flow velocity. In these figures, the propagation paths in blood vessels are set as  $d_{b1}$  and  $d_{b2}$ , respectively. The power spectra obtained from each depth can be expressed as Eqs. (7) and (8):

$$P_a(f, d_1) = \left| S(f, d_1)G(f)A(f, d_1)H(f, d_1)X(f) \right|^2, \tag{7}$$

$$P_a(f, d_2) = \left| S(f, d_2)G(f)A(f, d_2)H(f, d_2)X(f) \right|^2. \tag{8}$$

Here, assuming that the shear velocities at the positions of  $d_1$  and  $d_2$  are the same, because the positions are made an equal

distance from the center of the lumen,  $S(f, d_1)$  and  $S(f, d_2)$  are treated as the same. Taking the ratio of these two spectra and the logarithm gives the following equation:

$$10 \log_{10} \frac{P_a(f, d_1)}{P_a(f, d_2)} = 10 \log_{10} \frac{\left| \frac{A(f, d_1)}{A(f, d_2)} \right|^2}{\left| \frac{A(f, d_1)}{A(f, d_2)} \right|^2} + 10 \log_{10} \frac{\left| \frac{H(f, d_1)}{H(f, d_2)} \right|^2}{\left| \frac{H(f, d_1)}{H(f, d_2)} \right|^2}. \tag{9}$$

Equation (9) is converted into the following equation:

$$10 \log_{10} \frac{\left| \frac{A(f, d_1)}{A(f, d_2)} \right|^2}{\left| \frac{A(f, d_1)}{A(f, d_2)} \right|^2} = 10 \log_{10} \frac{P_a(f, d_1)}{P_a(f, d_2)} - 10 \log_{10} \frac{\left| \frac{H(f, d_1)}{H(f, d_2)} \right|^2}{\left| \frac{H(f, d_1)}{H(f, d_2)} \right|^2}. \tag{10}$$

The sound pressure property difference  $10 \log_{10} \left| \frac{H(f, d_1)}{H(f, d_2)} \right|^2 / \left| \frac{H(f, d_1)}{H(f, d_2)} \right|^2$  between the distances  $d_1$  and  $d_2$  in the second term on the right side of Eq. (10) is derived from the reflected waves from the underwater phantom and corrected. Therefore, the attenuation property difference  $10 \log_{10} \left( \left| \frac{A(f, d_1)}{A(f, d_2)} \right|^2 / \left| \frac{A(f, d_1)}{A(f, d_2)} \right|^2 \right)$  can be obtained by measuring  $P_a(f, d_1)$  and  $P_a(f, d_2)$ . The left side of Eq. (10) can be expressed as follows:

$$10 \log_{10} \frac{\left| \frac{A(f, d_1)}{A(f, d_2)} \right|^2}{\left| \frac{A(f, d_1)}{A(f, d_2)} \right|^2} = 10 \log_{10} \frac{\left| \frac{A_b(f, d_{b1})}{A_b(f, d_{b2})} \right|^2}{\left| \frac{A_b(f, d_{b1})}{A_b(f, d_{b2})} \right|^2}$$

$$= 20 \{ \log_{10} A_b(f, d_{b1}) - \log_{10} A_b(f, d_{b2}) \}$$

$$= 20 \{ \log_{10} e^{-2\alpha_b(f)d_{b1}} - \log_{10} e^{-2\alpha_b(f)d_{b2}} \}$$

$$= 17.37 (d_{b2} - d_{b1}) \alpha_b(f). \tag{11}$$

Therefore, the attenuation coefficient of blood  $\widehat{\alpha_b(f)}$  is obtained by the following equation:

$$\widehat{\alpha_b(f)} = \frac{1}{17.37 (d_{b2} - d_{b1})} \cdot 10 \log_{10} \frac{\left| \frac{A(f, d_1)}{A(f, d_2)} \right|^2}{\left| \frac{A(f, d_1)}{A(f, d_2)} \right|^2}. \tag{12}$$

Here, the propagation attenuation is caused by two factors, i.e., scattering and absorption. The attenuation coefficient of blood during avascularization ( $\alpha_b'(f)$ ) can be calculated in the same way.

**Size estimation method by fitting theoretical and measured properties**

In the present study, a scatterer was modeled by assuming an infinite number of infinitesimal point sources on the surface of a spherical scattering source [20]. The theoretical scattering property when the scatterer is irradiated by a plane wave is given by [21]

$$\frac{Q(ka)}{4\pi a^2} = \sum_{n=0}^{\infty} \frac{2n+1}{(ka)^2} \sin^2 [\delta'_n(ka)], \tag{13}$$

where  $Q(ka)$  is the scattering cross-section,  $k$  is the wave-number,  $a$  is the radius of the scatterer,  $n$  is the number of point sources on the surface of the scatterer, and  $\delta'_n(ka)$  is the derivative of the phase difference between the incident and scattered waves.

Obtaining a theoretical power that minimizes the sum of squares  $\epsilon(a, b)$  of the difference between the normalized power spectrum  $10 \log_{10} |S(f, d_0)|^2 / |R|^2$  obtained by the measurement and the theoretical scattering power spectrum for a single spherical scatterer (Fig. 2a) with different diameters at every 1  $\mu\text{m}$  considering the size of a single RBC [21], the size of the RBC aggregation is estimated [10]. It is shown in the following equation:

$$\epsilon(a, b) = \sum_{k=0}^{N-1} w(f_k) \left[ 10 \log_{10} \frac{|S(f_k, d_0)|^2}{|R|^2} - 10 \log_{10} \left\{ \frac{bQ(ka)}{4\pi a^2} \right\} \right]^2, \tag{14}$$

where  $w(f_k)$  is the weighting function and  $b$  is the intercept of the theoretical spectrum. In the conventional and proposed methods, the normalized power spectra  $10 \log_{10} |S(f, d_0)|^2 / |R|^2$  were obtained without and with consideration of the propagation attenuation component  $10 \log_{10} |A_s(f, d_0)|^2 / |A_r(f, d_0)|^2$  in Eq. (3), respectively. The weighting function  $w(f_k)$  is calculated from the amplitude of the scattered power  $P_s(f, d)$  obtained from RBCs. Since the power spectrum  $P_s(f, d)$  of the scatterer changes at each measurement, the weighting function  $w(f_k)$  is calculated at each measurement for estimating the scatterer size. Figure 2b shows the measured normalized power spectrum, the theoretical power spectrum that minimizes  $\epsilon$ , and the weighting function.

### Basic experiments using microparticles

To verify the accuracy of the proposed method, we experimented using microparticles with known sizes. The sizes of the microparticles were 5 and 20  $\mu\text{m}$  in diameter, and each aqueous solution with a microparticles volume ratio of 5, 7, and 10% was prepared in a beaker. To disperse the microspheres, polyxyethelene octylphenyl ether was used as the surfactant. The surface of the ultrasonic probe was inserted into the solution in a steady state. Using the Tomey Ultrasound Diagnostic System UD-8000 with a mechanical sector probe (center frequency: 40 MHz, wavelength: 38.5  $\mu\text{m}$ , focal point: 9 mm), 19 frames of RF signals were acquired every 5 s at a sampling frequency of 240 MHz. The number of beams was 113 per frame. The pairs of positions  $(d_1, d_2)$  of the window used for the attenuation calculation were set at three different positions, (A) (8.25: 9.75 mm), (B) (8.5: 9.5 mm), and (C) (8.75: 9.25 mm), which were the same distances from the depth of 9 mm to cancel out the scattering properties  $S(f, d_1)$  and  $S(f, d_2)$  in in vivo experiments. Each window width was 240  $\mu\text{m}$ . The propagation attenuation components were calculated at each frame using the attenuation coefficient calculated at each frame, and the particle sizes were estimated using both the conventional method without correcting the propagation attenuation component and the proposed method with the correction.

### In vivo measurements

RBC aggregation is likely to occur at low shear rates [13, 22, 23]. Therefore, a situation in which RBC aggregation was likely to occur by avascularizing and reducing blood flow was modeled in addition to without avascularization. RF signals from blood were obtained when RBCs were aggregated and not aggregated. The measurement target was the dorsal vein near the skin. RF signals were acquired at a sampling frequency of 240 MHz using a Tomey UD-8000

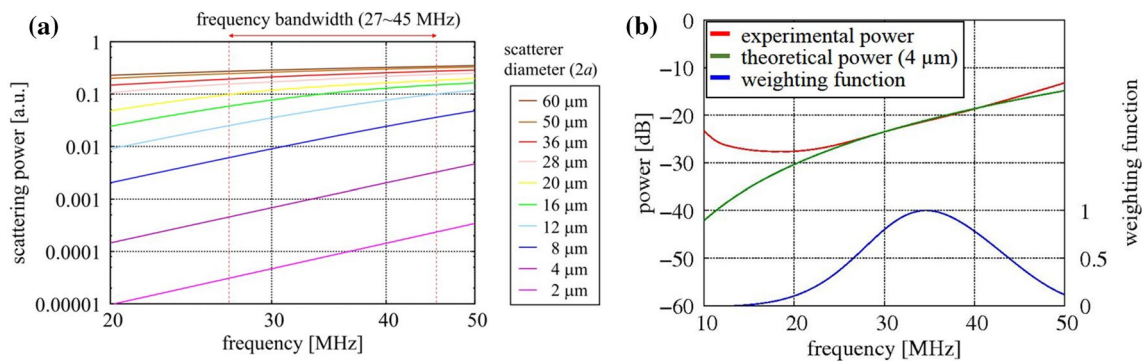


**Fig. 2** Size estimation by fitting theoretical and measured scattering properties. **a** Theoretical properties for each scatterer size [19]. **b** Fitting results for theoretical and measured properties with a weighting function

ultrasound system (center frequency: 40 MHz, wavelength: 38.5  $\mu\text{m}$ , focal point: 9 mm). The measurement procedure was as follows. First, the posterior wall of the vein was set at a depth of 9 mm, and RF echoes from the lumen-intima interface were acquired. Then, setting the center of the vascular lumen to a depth of 9 mm, we measured a total of 19 frames; 7 frames every 10 s before avascularization and 12 frames every 10 s during avascularization. The propagation attenuation component was calculated at each frame using the attenuation coefficient calculated at each frame, and the aggregation sizes were estimated without and with correction of the propagation attenuation components. The power spectra were calculated for 339 RF signals obtained from 113 beams with Hanning windows of 240  $\mu\text{m}$  at three different positions in the lumen, and they were averaged. The central window was set to a depth of 9 mm, and the remaining two windows were set to a depth shifted up or down by 120  $\mu\text{m}$  from the focal depth for each beam. The subjects were two healthy males.

## Results and discussion

### Basic experiments using microparticles

The attenuation coefficients were measured for three solutions; 5- $\mu\text{m}$  and 20- $\mu\text{m}$  microparticles were dissolved, respectively, in two solutions, and they were mixed at a ratio of 1:1 in a solution. Figure 3 shows B-mode images of each solution at a 5% volume ratio, power spectra, and the attenuation coefficients  $\alpha_m(f)$  calculated with windows at positions (A) (8.25: 9.75 mm), (B) (8.5: 9.5 mm), and (C) (8.75: 9.25 mm). As shown in Fig. 3, the attenuation coefficients  $\alpha_m(f)$  increased as the size increased. Comparing the attenuation coefficients at different window positions with the three solutions, similar properties were exhibited at positions (A) and (B), but the slope at position (C) was steeper than those at positions (A) and (B). This suggests that the calculation of the attenuation coefficient requires sufficient distance between two windows.

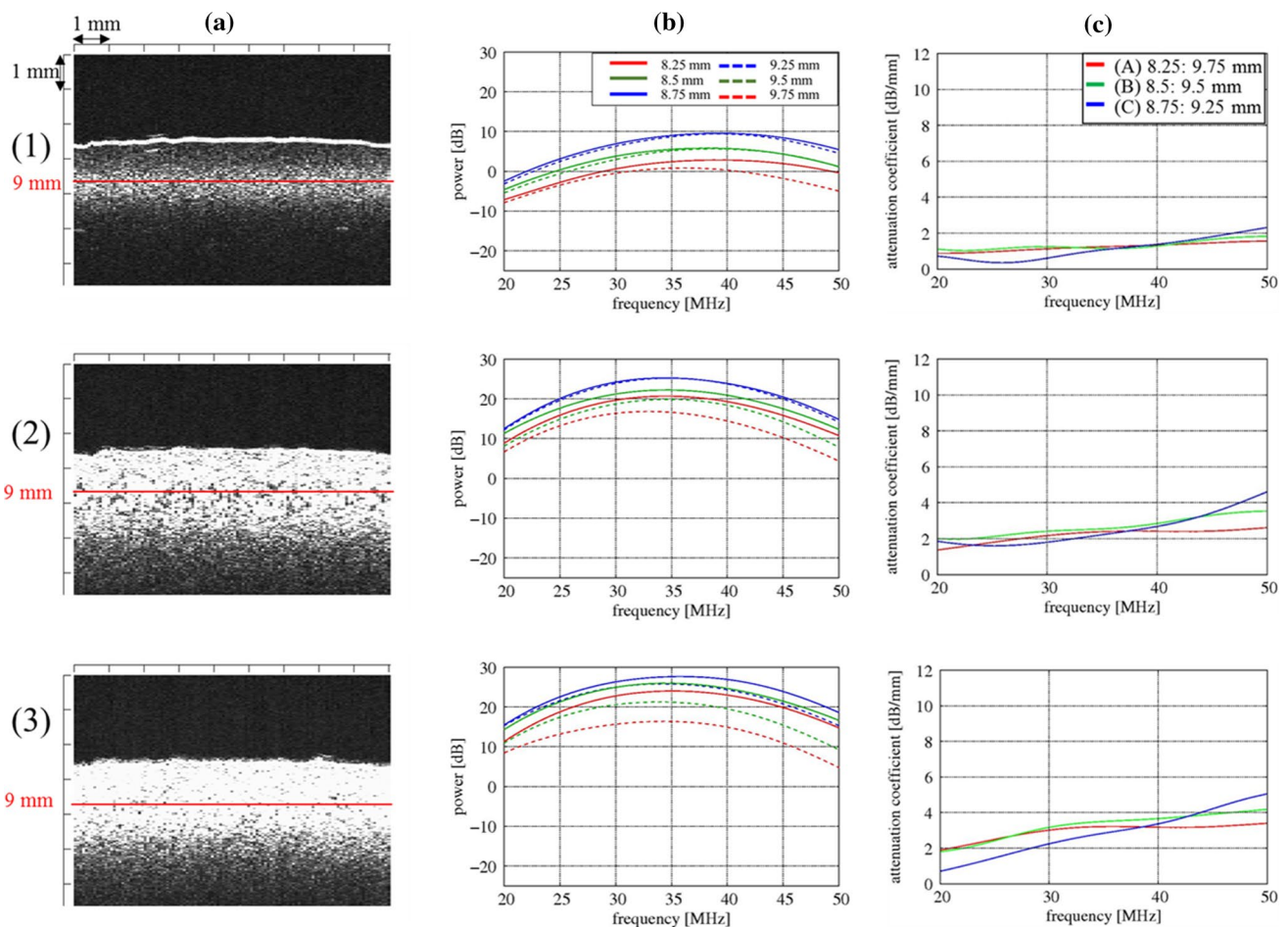
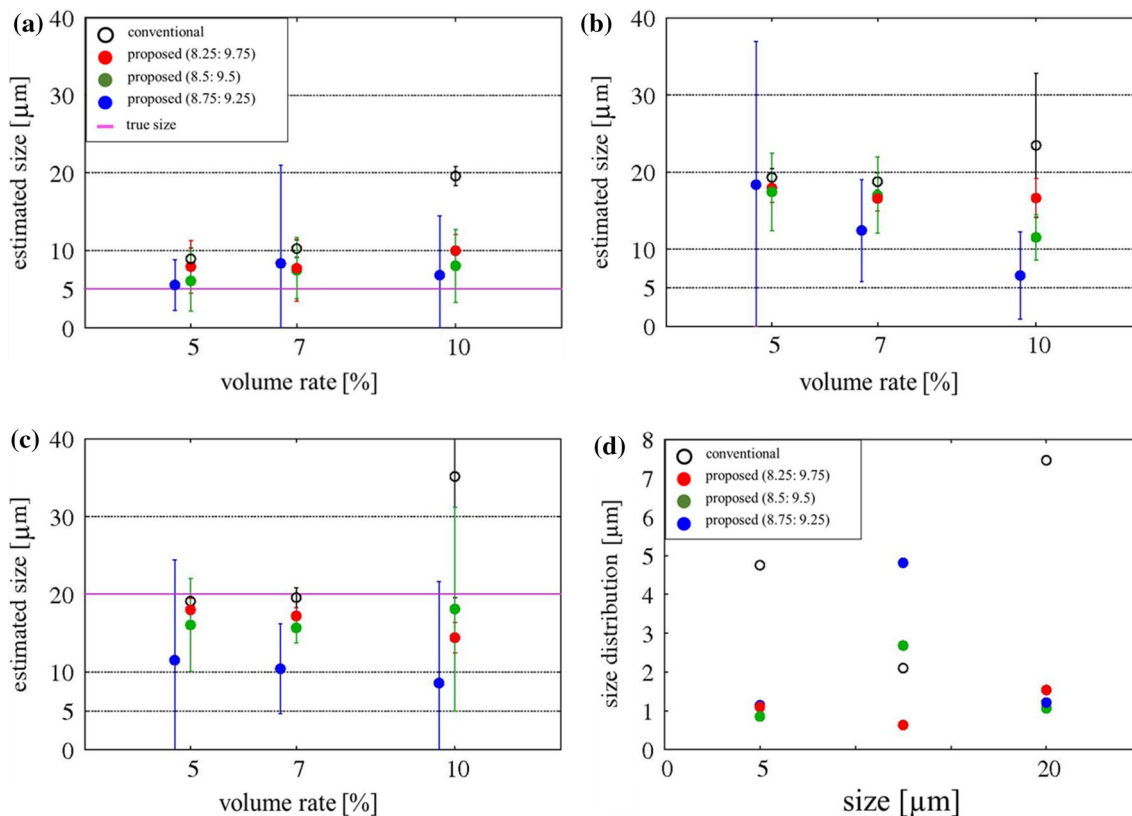


**Fig. 3** B-mode images and attenuation coefficients for microparticles. **a** B-mode image. **b** Power spectrum. **c** Attenuation coefficient  $\alpha_m(f)$ . (1) 5  $\mu\text{m}$ . (2) Mixed with 5  $\mu\text{m}$  and 20  $\mu\text{m}$ . (3) 20  $\mu\text{m}$

Figure 4 shows the size estimation results. With the conventional method, the estimated size increased as the volume ratio increased for all particle sizes. It was considered that the higher the volume ratio, the higher the attenuation caused by the scattering in the propagation path, remarkably in the higher-frequency components. It caused the slope of the spectrum to become gentler, and the size was estimated to be large. With the estimation using the proposed method, almost the same sizes were estimated regardless of the volume ratio for 5- $\mu\text{m}$  particles, and they were closer to the true size compared to the conventional method. It was also shown that the proposed method gave almost the same sizes regardless of the volume ratio change even in the solution in which the two kinds of particles were mixed and the 20- $\mu\text{m}$  particle solution with window positions (A) and (B). For 20- $\mu\text{m}$  particles, the sizes estimated with the proposed method were slightly smaller than 20  $\mu\text{m}$  with window positions (A) and (B). When we observed a 20- $\mu\text{m}$  microparticle solution using an optical microscope, it was confirmed that the particle sizes were approximately ranged from 15 to 22  $\mu\text{m}$ . Therefore, the particle sizes were estimated to be

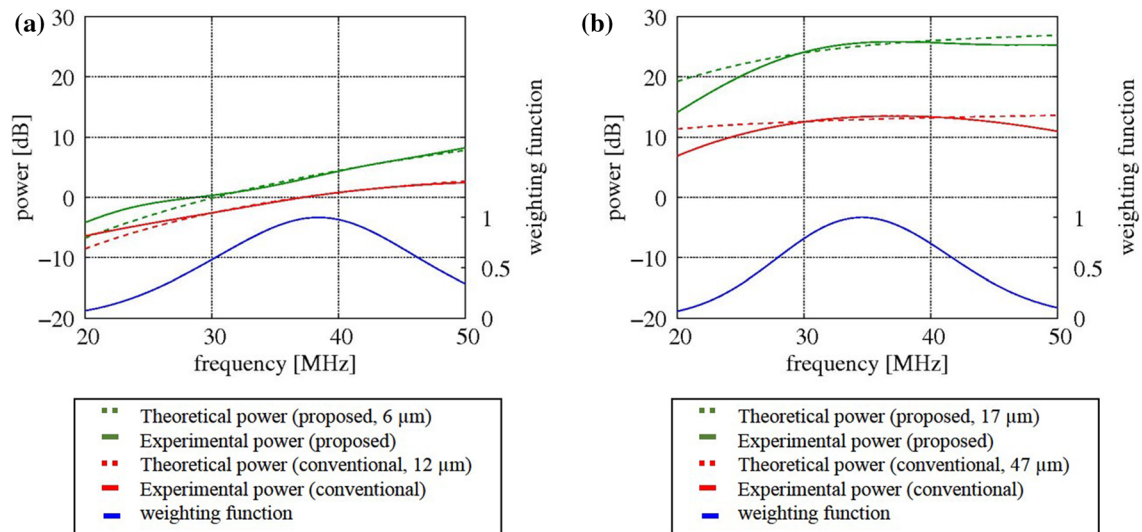
smaller than 20  $\mu\text{m}$  with the proposed method, but it could be within a reasonable range. The variations of the estimated sizes became large with window position (C). This suggests that the accuracy of the estimated attenuation coefficient obviously affects the accuracy of the estimated size. With the proposed method, the attenuation coefficient was estimated at each frame. Therefore, the variations of the estimated sizes became larger than those yielded by the conventional method caused by the variations of the estimated attenuation coefficients.

Figure 5 shows examples of the size estimation fitted with the conventional method and the proposed one. With the proposed method, the slope of the measured spectrum was steeper than that obtained by the conventional method, and the estimation size was smaller than that estimated by the conventional method. It was possible to estimate a value close to the true size with the proposed method regardless of the volume ratio or the particle size, and it was demonstrated that the estimation accuracy of the particle size was improved. Moreover, it was also demonstrated that the attenuation coefficients  $\alpha_m(f)$  could be properly estimated.



**Fig. 4** Size estimation results for microparticles. **a** 5  $\mu\text{m}$ . **b** Mixed with 5  $\mu\text{m}$  and 20  $\mu\text{m}$ . **c** 20  $\mu\text{m}$ . **d** Variation in the estimated sizes for different volume ratios. The estimated results with the window at

position (C) (8.75: 9.25 mm) were plotted shifted left in the  $x$  direction in **a–c**. The results for the mixed solution were plotted at 12.5  $\mu\text{m}$  for convenience



**Fig. 5** Fitting results of measured and theoretical scattering properties using the conventional and proposed methods. (a) 5  $\mu\text{m}$ . (b) 20  $\mu\text{m}$

### In vivo measurements

In blood vessels, the blood flow at the center of the blood vessel is faster than that near the wall due to the effect of laminar flow. Since RBC aggregation is more likely to occur as blood flow is slower, it is necessary to set the analysis window at a position at which the blood flow velocity is the same when calculating the attenuation coefficients. The measurement depth  $d_0$ , which corresponds to the center of the lumen, was set at 9 mm, and the attenuation coefficients  $\alpha_b(f)$  and  $\alpha'_b(f)$  were calculated with windows at positions (8.25: 9.75 mm), at which the estimation result was the most accurate in the basic experiment using microparticles. Figure 6 shows the B-mode images and the attenuation coefficients  $\alpha_b(f)$  and  $\alpha'_b(f)$  of subject A before and during avascularization. The 0th–6th frames before avascularization and 12th–18th frames during avascularization were averaged, and the error bars were the standard deviations among these seven frames. The red and blue frames in the B-mode images indicate the window positions (8.25: 9.75 mm). From these B-mode images, it can be confirmed that RBC aggregation occurred during avascularization, the brightness of the lumen increased, and the attenuation coefficient got larger. The slope of frequency characteristics of attenuation coefficients became larger during avascularization in the frequency bandwidth of 27–45 MHz of the ultrasound probe used in the measurements.

Figure 7 shows the results of RBC size estimation using the conventional method and the proposed method for subjects A and B. The results estimated with the conventional method and the proposed method corrected by the attenuation coefficient at each frame are indicated by red circles

and green triangles, respectively. The averaged attenuation coefficients, which were obtained for the 0th–6th frames before avascularization and the 12th–18th frames during avascularization, as shown in Fig. 6, were also used for the proposed method for the 0th–6th frames and 12th–18th frames, respectively, and the results are shown in Fig. 7 with blue inverted triangles. The averaged attenuation coefficients were not used for the 7th–11th frames, because the attenuation coefficient varied with elapsed time from the beginning of the avascularization. When the attenuation coefficient was corrected at each frame, the size variation at each frame became large. However, when the averaged attenuation was used for the correction, the variations were reduced. The average estimated sizes and the standard deviations with correction using the averaged attenuation coefficients and without correction are summarized in Table 1. Significant size differences between at rest and during avascularization were not obtained between with and without attenuation correction in spite of using the averaged attenuation coefficient. It might be caused by the fact that the variation of the spectra was large even though 339 spectra were averaged. In the future, we will discuss a method to correct the propagation attenuation component more accurately by selecting the beams at averaging of the power spectra and using multiple points such as attenuation imaging [24].

Acquisition of reproducible data with our method in vivo is another issue to solve, because the data depend on blood glucose status, blood flow, and so on. Moreover, it is important to increase the sample size to investigate the reproducibility and demonstrate the usefulness of the size estimation method.

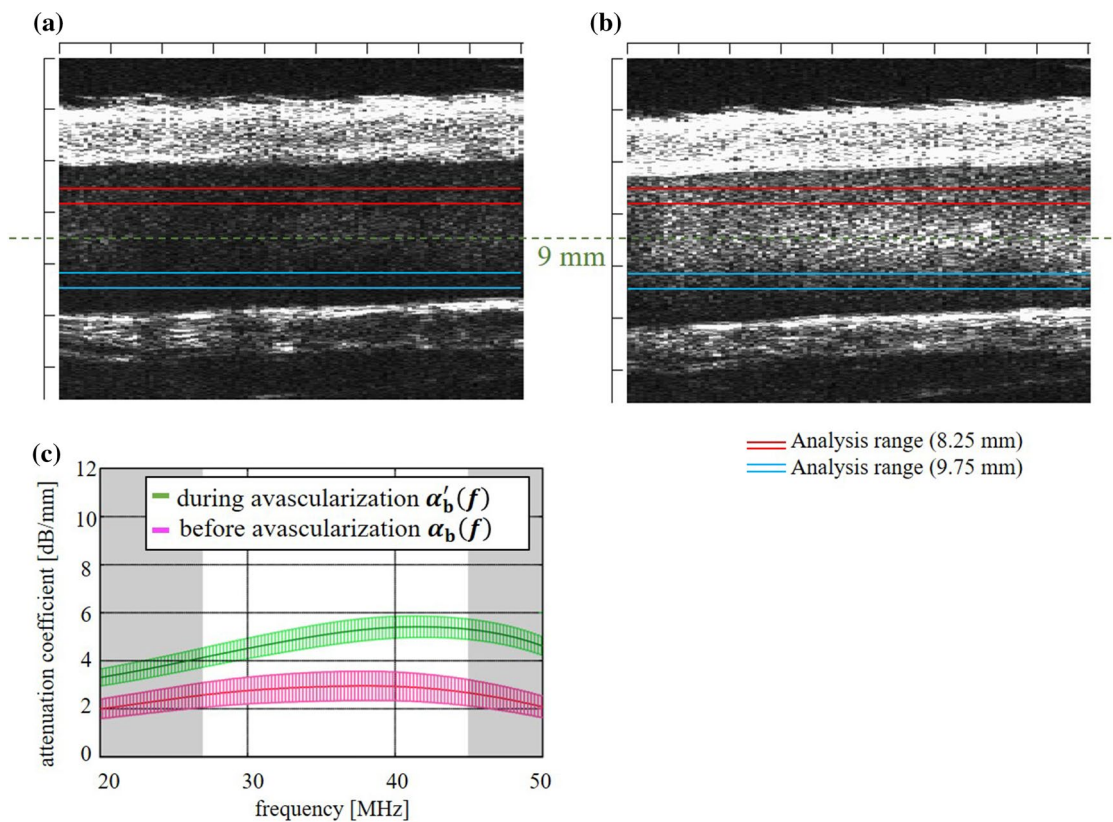


**Fig. 6** B-mode images and attenuation coefficients in in vivo measurement. **a** B-mode image (before avascularization). **b** B-mode image (during avascularization). **c** Attenuation coefficients  $\alpha_b(f)$  and  $\alpha'_b(f)$

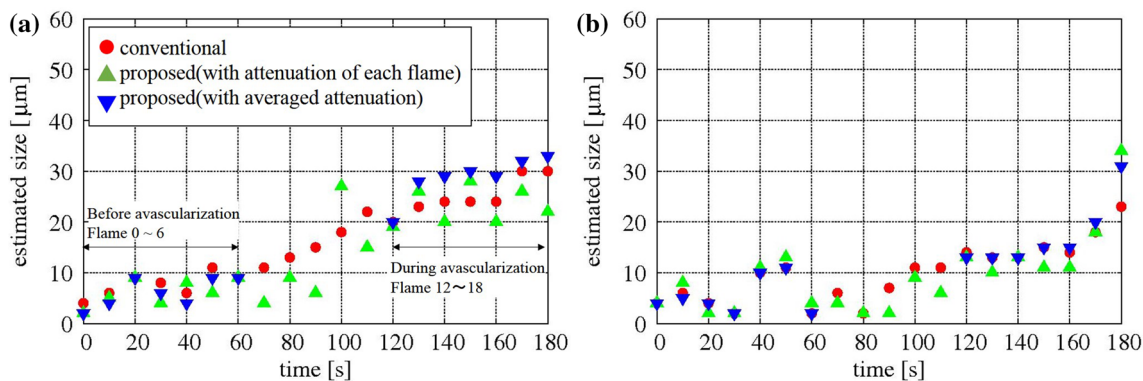


**Fig. 7** Size estimation results in in vivo measurements. **a** Subject A. **b** Subject B

**Table 1** Size estimation results in in vivo measurements. Values in parentheses are the standard deviation

	At rest (0th–7th frames)		Avascularization (12th–18th frames)	
	Without correction	With correction	Without correction	With correction
Subject A	7.6 (2.2)	6.1 (2.7)	25.0 (3.4)	28.7 (3.9)
Subject B	5.6 (3.4)	5.4 (3.4)	15.7 (3.4)	17.1 (6.1)

## Conclusion

In the present study, we tried to improve the accuracy of the size estimation method by deriving the intravascular ultrasonic propagation attenuation and correcting the propagation attenuation component.

When the attenuation coefficient was calculated in an measurement using microparticles, it was confirmed that the attenuation coefficient increased as the particle size and the volume ratio increased. The attenuation coefficient could be calculated precisely when the distance between windows was long. In the case of the conventional method, the size estimation accuracy became worse as the volume ratio became higher. By removing the propagation attenuation component using the proposed method, it was possible to estimate it with a nearly constant value regardless of the change in the volume ratio, which suggested that the proposed method could stably estimate the size regardless of differences in hematocrit levels or the degree of RBC aggregation. In in vivo measurement, significant differences could not be obtained with and without the attenuation correction. This might have been caused by the large variation in the measured spectra. Going forward, we will investigate a method to correct the propagation attenuation component more accurately.

**Acknowledgements** This work was partly supported by JSPS KAKENHI through Grant no. 19K22943.

## Compliance with ethical standards

**Conflict of interest** The authors have no conflicts of interest concerning the presented research.

**Ethical statement** Informed consent to the protocol was obtained from control subjects. The study was approved by our institutional ethics committee for human research.

## References

- Paeng DG, Chiao RY, Shung KK. Echogenicity variations from porcine blood II: the “bright ring” under oscillatory flow. *Ultrasound Med Biol.* 2004;30:815–25.
- Huang CC, Wang SH. Characterization of blood properties from coagulating blood of different hematocrits using ultrasonic backscatter and attenuation. *Jpn J Appl Phys.* 2006;45:7191–6.
- Ikemoto S, Kuchiba K, Akiyama M, et al. Elevated viscoelasticity of blood in diabetic microangiopathy. *J Jpn Diabetes Soc.* 1988;31:231–7.
- Yoshida T, Sato K, Kondo T. Blood-mimicking fluid using glycols aqueous solution and their physical properties. *Jpn J Appl Phys.* 2014;53:07KF01-1–5.
- Takahashi H, Hasegawa H, Kanai H. Echo speckle imaging of blood particles with high-frame-rate echocardiography. *Jpn J Appl Phys.* 2014;53:07KF08-1–7.
- Paeng DG, Nam KH, Shung KK. Cyclic and radial variation of the echogenicity of blood in human carotid arteries observed by harmonic imaging. *Ultrasound Med Biol.* 2010;36:1118–24.
- Paeng DG, Nam KH, Choi MJ, et al. Three-dimensional reconstruction of the ‘bright ring’ echogenicity from porcine blood upstream in a stenosed tube. *IEEE Trans Ultrason Ferroelectr Freq Control.* 2009;56:880–5.
- Libgot-Callé R, Ossant F, Gruel Y, et al. High frequency ultrasound device to investigate the acoustic properties of whole blood during coagulation. *Ultrasound Med Biol.* 2008;34:252–64.
- Callé R, Plag C, Patat F, et al. Interest of the attenuation coefficient in multiparametric high frequency ultrasound investigation of whole blood coagulation process. *J Acoust Soc Am.* 2009;125:530–8.
- Saitoh N, Hasegawa H, Kanai H. Estimation of scatterer diameter using ultrasonic backscattering property for assessment of red blood cell aggregation. *Jpn J Appl Phys.* 2009;48:07GJ08-1–5.
- Fukushima T, Hasegawa H, Kanai H. Estimation of scatterer diameter by normalized power spectrum of high-frequency ultrasonic RF echo for assessment of red blood cell aggregation. *Jpn J Appl Phys.* 2011;50:07HF02-1–8.
- Kurokawa Y, Taki H, Yashiro S, et al. Estimation of size of red blood cell aggregates using backscattering property of high-frequency ultrasound: In vivo evaluation. *Jpn J Appl Phys.* 2016;55:07KF12-1–8.
- Miwa S. Sekkekkyu. Igaku-Shoin, Tokyo; 1998, pp. 60–9 (in Japanese).
- Baldwin SL, Marutyan KR, Yang M, et al. Estimating myocardial attenuation from M-mode ultrasonic backscatter. *Ultrasound Med Biol.* 2015;31:477–84.
- Chen J, Hou GY, Marquet F, et al. Radiation-force-based estimation of acoustic attenuation using harmonic motion imaging (HMI) in phantoms and in vitro livers before and after HIFU ablation. *Phys Med Biol.* 2015;60:7499–512.
- Kim H, Varghese T. Attenuation estimation using spectral cross-correlation. *IEEE Trans Ultrason Ferroelectr Freq Control.* 2007;54:510–9.
- Heo SW, Kim H. A novel power spectrum calculation method using phase-compensation and weighted averaging for the estimation of ultrasound attenuation. *Ultrasonics.* 2010;50:592–9.
- Kuc R. Bounds on estimating the acoustic attenuation of small tissue regions from reflected ultrasound. *Proc IEEE.* 1985;73:1159–68.
- Hashimoto Y, Akashi N, Kushibiki J. Measurements of ultrasonic attenuation coefficients of water in VHF/UHF range. *Tech Rep IEICE.* 1997;97:37–42.
- Fontaine I, Cloutier G. Modeling the frequency dependence (5–120 MHz) of ultrasound backscattering by red cell aggregates in shear flow at a normal hematocrit. *J Acoust Soc Am.* 2003;113:2893–900.
- Morse PM, Feshbach H. *Methods of theoretical physics.* New York: McGraw-Hill; 1953.
- Yagi S, Nakayama K. Acoustic scattering in weakly inhomogeneous dispersive media: experimental analysis. *Acoust Soc Jpn.* 1983;39:659–67.
- Yagi S, Nakayama K. Absolute measurement of scattering characteristics of dispersive media using ultrasonic wideband pulse. *Acoust Soc Jpn.* 1987;43:777–85.
- Tada T, Iijima H, Kobayashi N, et al. Usefulness of attenuation imaging with an ultrasound scanner for the evaluation of hepatic steatosis. *Ultrasound Med Biol.* 2019;45:2679–87.

**Publisher’s Note** Springer Nature remains neutral with regard to jurisdictional claims in published maps and institutional affiliations.